Arteriosclerosis, Thrombosis, and Vascular Biology

BASIC SCIENCES

Inhibition of Vascular Growth by Modulation of the Anandamide/Fatty Acid Amide Hydrolase Axis

Sarah Rieck,* Sofia Kilgus,* Johanna H. Meyer, Hao Huang, Lan Zhao, Michaela Matthey, Xin Wang, Steffen Schmitz-Valckenberg, Bernd K. Fleischmann, Daniela Wenzel

OBJECTIVE: Pathological angiogenesis is a hallmark of various diseases characterized by local hypoxia and inflammation. These disorders can be treated with inhibitors of angiogenesis, but current compounds display a variety of side effects and lose efficacy over time. This makes the identification of novel signaling pathways and pharmacological targets involved in angiogenesis a top priority.

APPROACH AND RESULTS: Here, we show that inactivation of FAAH (fatty acid amide hydrolase), the enzyme responsible for degradation of the endocannabinoid anandamide, strongly impairs angiogenesis in vitro and in vivo. Both, the pharmacological FAAH inhibitor URB597 and anandamide induce downregulation of gene sets for cell cycle progression and DNA replication in endothelial cells. This is underscored by cell biological experiments, in which both compounds inhibit proliferation and migration and evoke cell cycle exit of endothelial cells. This prominent antiangiogenic effect is also of pathophysiological relevance in vivo, as laser-induced choroidal neovascularization in the eye of *FAAH*$^{-/-}$ mice is strongly reduced.

CONCLUSIONS: Thus, elevation of endogenous anandamide levels by FAAH inhibition represents a novel antiangiogenic mechanism.

GRAPHIC ABSTRACT: A graphic abstract is available for this article.

Key Words: anandamide ■ choroidal neovascularization ■ endothelial cell ■ fatty acid amide hydrolase ■ inflammation

Angiogenesis plays an important role in health and disease. In the adult organism, new vessels only develop in special organs or situations, for example, during reproduction,[1] hair growth,[2] and wound healing.[3] Insufficient vessel growth is involved in ischemic diseases such as myocardial infarction and stroke,[4] whereas excessive angiogenesis supports retinal disorders,[5] tumor growth, and inflammatory diseases.[6] Therefore, a better understanding of the mechanisms underlying angiogenesis could lead to novel therapeutic targets. Vasoactive agents such as VEGF (vascular endothelial growth factor) and endostatin often proved to affect both vascular tone and angiogenesis.[7,8] Recently. we identified the enzyme FAAH (fatty acid amide hydrolase) as a key mediator of hypoxic pulmonary vasoconstriction. We found that hypoxia induces the generation of the endocannabinoid anandamide (AEA) in smooth muscle cells, and this is metabolized by FAAH to vasoconstrictive eicosanoids causing the induction of hypoxic pulmonary vasoconstriction.[9] Therefore, we wondered if modulation of FAAH could also affect vascular growth. FAAH is the main degradation enzyme of AEA which was first identified as a neurotransmitter influencing appetite,[10] memory,[11] and pain sensation.[12] Later, it was found that endocannabinoids can be also produced by endothelial

Correspondence to: Daniela Wenzel, MD, Institute of Physiology, Department of Systems Physiology, Medical Faculty, University of Bochum, Universitätsstr. 150, 44801 Bochum, Germany. Email daniela.wenzel@rub.de
*S. Rieck and S. Kilgus contributed equally.
The Data Supplement is available with this article at https://www.ahajournals.org/doi/suppl/10.1161/ATVBAHA.121.316973.
For Sources of Funding and Disclosures, see page 2987.

Nonstandard Abbreviations and Acronyms

AEA	anandamide
CNV	choroidal neovascularization
DPBS	Dulbecco's PBS
EB	embryoid body
EC	endothelial cell
eGFP	enhanced green fluorescence protein
ES	embryonic stem
FAAH	fatty acid amide hydrolase
HUVEC	human umbilical vein endothelial cell
ICAM2	intercellular cell adhesion molecule 2
Met-AEA	methanandamide
VEGF	vascular endothelial growth factor

cells (EC) and display vasoactive properties.[13] In fact, endocannabinoid-related compounds were reported to induce vasorelaxation[14] or vasoconstriction[9,15] in different vascular beds via different molecular mechanisms. Although there are hints in the literature that endocannabinoids could affect angiogenesis, it remains unclear, if they stimulate[16] or decrease vascular growth.[17] In particular, the role of the enzyme FAAH in vascularization is still completely unknown. Therefore, in the current study, we investigated the impact of FAAH inhibition on angiogenesis in vitro and in vivo.

Highlights

- Inhibition of FAAH (fatty acid amide hydrolase), the main enzyme that degrades the endocannabinoid anandamide, diminishes vascular growth.
- This effect is mediated by anandamide accumulation and direct interaction with lipid membranes.
- FAAH-deficient mice are protected from laser-induced choroidal neovascularization which phenocopies wet age-related macular degeneration in humans.

MATERIALS AND METHODS

All data for this study are available from the corresponding author upon reasonable request.

The gene array data are available at GEO (National Institutes of Health) under the accession number GSE152552.

Cultivation and Treatment of EC Lines, Smooth Muscle Cells as well as Fibroblasts

All cell lines were cultivated under sterile conditions at 37 °C in a humidified atmosphere with 5% CO_2. Human umbilical vein ECs (HUVEC; Provitro, Berlin, Germany) and bovine pulmonary artery ECs (Cell Applications, San Diego) were cultivated in EC growth medium (final FCS concentration 2%; Provitro). Human microvascular ECs derived from lung (Provitro) were cultivated in microvascular EC growth medium (final FCS concentration 5%; Provitro). Human aortic smooth muscle cells (Lonza, Basel, Switzerland) were cultivated in Medium 231 (final FCS concentration: 5%; Life technologies). Human lung fibroblasts 1 were cultivated in DMEM (FCS concentration 10%). All media were supplemented with 1% (v/v) penicillin/streptomycin (Life Technologies, Darmstadt, Germany). All cell lines were allowed to grow until a confluency of 80% was reached. Then, the ECs were detached using Accutase (Merck Millipore), other cell lines were treated with trypsin (Life technologies) and seeded at different densities for experiments. Cells were treated for 24 hours unless otherwise stated.

Angiogenesis Assay Using flt1/Enhanced Green Fluorescence Protein Embryonic Stem Cells

For an embryonic stem (ES) cell–based angiogenesis assay *flt1* (fms-like tyrosine kinase 1)*/eGFP* (enhanced green fluorescence protein) ES cells were used.[18,19] Undifferentiated murine *flt1/eGFP* ES cells were cultivated in growth medium (DMEM; Life Technologies) supplemented with 15% (v/v) FCS (PAN Biotech, Aidenbach, Germany), 1% (v/v) penicillin/streptomycin, 1% (v/v) nonessential amino acids (Life Technologies), 0.1% (v/v) β-mercaptoethanol (Sigma Aldrich, Taufkirchen, Germany), 1000 units/mL LIF (leukemia inhibitory factor; Merck Millipore), 300 µg/mL neomycin (Life technologies) under sterile conditions at 37 °C in a humidified atmosphere with 5% CO_2. Irradiated and neomycin-resistant mouse fibroblasts (Merck Millipore) were used as feeder cells. For differentiation of *flt1/eGFP* ES cells, the mass culture method was used. Therefore, 2 000 000 cells were seeded in a petri dish containing 10 mL differentiation medium (Iscove's Modified Dulbecco's Medium (Life Technologies) supplemented with 20% [v/v] FCS plus additives), and cells were agitated with 80 rpm for 3 days until embryoid bodies (EBs) had been formed. The mass culture was diluted (750 EBs in 10 mL differentiation medium/petri dish) and further agitated for seven days. At day ten of differentiation, EBs were dissociated. Therefore, 1500 EBs were transferred to a reaction tube and washed twice with Dulbecco's PBS (DPBS; Life technologies). Then, DPBS was replaced by dissociation buffer (Hank's balanced salt solution without Mg^{2+} and Ca^{2+} ($HBSS^{-/-}$; Life Technologies) supplemented with 280 units/mL collagenase IV (Worthington, Lakewood) and 1 µmol/L $CaCl_2$ and the EBs were agitated with 800 rpm for 10 minutes at 37 °C. Then, the supernatant containing single cells was transferred to differentiation medium (see above). Digestion and transfer of supernatant were repeated twice. After centrifugation (1000 rpm, 5 minutes), 1 000 000 cells per well were seeded in 2 mL differentiation medium in a 6-well plate coated with 0.1% (w/v) gelatin and differentiated for 10 days (day ten of differentiation+10). Medium was changed every day. Twenty-four hours after dissociation (day ten of differentiation+1) cells were treated with URB597 (10 µmol/L, Cayman Chemical, Ann Arbor), N-nitro-L-arginine methyl ester hydrochloride (10 µmol/L; Sigma Aldrich), AEA (10 µmol/L; Tocris Bioscience, Bristol, United Kingdom) or methanandamide (Met-AEA, 5 µmol/L; Cayman Chemical, Ann Arbor) in differentiation medium. The treatment was continued until day ten of differentiation+10. Then, network formation was documented with an Axiovert 200 M microscope (Zeiss, Jena, Germany).

Matrigel-Based Angiogenesis Assays

A Matrigel assay was performed as described earlier.[20,21] BD Matrigel (BD Biosciences, Heidelberg, Germany) was thawed according to the manufacturer`s instruction. A 24-well plate was kept at 4 °C overnight, and on the next day, it was coated with 250 µL matrigel/well. After Matrigel had polymerized in an incubator, 60 000 HUVEC were treated with solvent, URB597 (10 µmol/L, 20 µmol/L, 50 µmol/L, 100 µmol/L), AEA (10 µmol/L), or Met-AEA (5 µmol/L) for 24 hours or 10 mmol/L methyl-beta-cyclodextrin (MβC; Sigma Aldrich) for 1 hour and seeded on top of the polymerized BD Matrigel. Network formation was assessed 24 hours after seeding using an Axiovert 200 M microscope (Zeiss).

Endocannabinoid Measurements by Liquid Chromatography-Multiple Reaction Monitoring

HUVEC were treated with URB597 (20 µmol/L) or the solvent dimethyl sulfoxide (DMSO) in serum-free medium. After 24 hours, cells were harvested, transferred to Precelly Tubes (Precellys 24; Bertin Technologies), and centrifuged at 2000*g* for 10 minutes at 4 °C. The supernatant was discarded, and the cell pellet was frozen at −80 °C. Endocannabinoids were quantified by liquid chromatography-multiple reaction monitoring, as previously described.[9]

Aortic Ring Sprouting Assay

The assay was performed as described elsewhere.[22] Briefly, aortic rings from C57BL/6J wild-type and *FAAH*$^{-/-}$ mice were incubated for 24 hours in a humidified atmosphere with 5% CO_2 in Opti-MEM (Life Technologies) supplemented with 1% (v/v) penicillin/streptomycin (Life technologies) and were embedded in collagen gels afterward. The polymerized gel was covered with Opti-MEM containing 2% (v/v) FCS (PAN Biotech) and 1% (v/v) penicillin/streptomycin. The medium was exchanged every third day. For analysis phase-contrast images were taken at day 8 using an Axiovert 200 M microscope (Zeiss) and the number of sprouts per ring was counted.

Lentiviral Transduction

For transduction experiments lentivirus containing the pGFP-C backbone and an expression cassette with a small hairpin sequence for human fatty acid amide hydrolase or a nonsilencing control sequence, both driven by the U6 promoter were chosen (TL313109V, Amsbio, Abingdon, United Kingdom).

HUVECs were seeded on coverslips in a 24-well plate with a density of 20 000 cells/well. Twenty-four hours later, cells were transduced overnight with a multiplicity of infection of 2.5. Three days after transduction cells were fixated with 4% (w/v) paraformaldehyde and stained with anti-Ki67 antibody.

Analysis of Proliferation, Migration, and Apoptosis

For quantification of proliferation HUVEC or human aortic smooth muscle cells were seeded on coverslips and treated with URB597 (20 µmol/L), AEA (10 µmol/L), Met-AEA (5 µmol/L), arachidonic acid (10 M), oeloylethanolamide (10 µµmol/L), or palmitoylethanolamide (10 µ) for 24 hours or with 10 mmol/L MβC for 1 hour and then incubated in medium for additional 23 hours. Afterward, they were fixated with 4% (w/v) paraformaldehyde and stained with anti-Ki67 antibody as described before.[23,24]

To analyze migration of HUVEC a wound healing assay was performed. Three hundred thousand cells per well were seeded in a 6-well plate and cultivated until they reached 100% confluency. Then, URB597 (20 µmol/L) or AEA (10 µmol/L) were applied to the medium and a scratch was created in the cell monolayer using a pipet tip. In case of treatment with MβC cells were preincubated with 10 mmol/L MβC in medium for 1 hour, then medium was changed and the monolayer was scratched with a pipet tip. Time-lapse analysis of 3 different positions using an Axiovert 200 M microscope (Zeiss) was performed for 24 hours. Pictures were taken every 15 minutes. Wound healing was quantified as (mean scratch diameter at 0 hour−mean scratch diameter at 8 hours)/(mean scratch diameter after 0 hour).

Apoptosis of native HUVEC or HUVEC treated with URB597 (20 µmol/L), AEA (10 µmol/L), or MβC (10 mmol/L) was analyzed by flow cytometry using an AnnexinV-fluorescein isothiocyanate (FITC) apoptosis detection kit (Merck Millipore). As positive control, HUVEC were cultivated for 24 hours in the absence of serum.

Cell Cycle Analysis

HUVEC were treated with 20 µmol/L URB597 or 10 µmol/L AEA for 24 hours, washed once with DPBS, and then detached with Accutase. After centrifugation (1000 rpm, 5 minutes), they were fixated with ice-cold 80% (v/v) ethanol at −20 °C for 2 hours. Fixated cells were centrifuged for 10 minutes at 1000 rpm, washed with DPBS, and incubated with 100 µg/mL RNase A (Life Technologies) for 15 minutes at 37 °C. Then, propidium iodide solution (Sigma Aldrich) at a concentration of 50 µg/mL was applied, and flow cytometric analysis was performed.

Immunofluorescence Stainings

Immunofluorescence stainings were exerted as described recently.[25] HUVEC and human aortic smooth muscle cells were fixated with 4% (w/v) paraformaldehyde and permeabilized with 0.2% (v/v) TritonX-100. After blocking of unspecific binding sites with 5% (w/v) donkey serum (Jackson ImmunoResearch, Suffolk, United Kingdom) for 30 minutes, cells were incubated with primary antibody for 1 hour. Following primary antibodies were used: anti-FAAH (rabbit, 1:50, Cayman Chemicals), anti-Ki67 (mouse, 1:200; Dako, Hamburg, Germany). Next, Cy3-labeled anti-mouse or anti-rabbit secondary antibody F (Jackson ImmunoResearch) was applied for 1 hour. Nucleus staining was performed with Hoechst (1:1000; Sigma Aldrich). For the staining of lipid rafts, HUVEC were seeded on coverslips and treated for 1 hour with MβC (10 mmol/L) and then incubated in medium for additional 23 hours, alternatively, incubation for 24 hours was performed with ethanol as solvent, URB597 (20 µmol/L), AEA (10 µmol/L), arachidonic acid (10 µmol/L), oleoylethanolamide (oeloylethanolamide, 10 µmol/L), palmitoylethanolamide (10 µmol/L), or Met-AEA (5 µmol/L). Then, the cell culture dish was placed on ice, cells were washed 3× with ice-cold DPBS, and fixated with paraformaldehyde for 15 minutes at 4 °C. Fixated cells were blocked for 30 minutes with 5% (v/v) donkey serum in DPBS. Then, staining

of lipid rafts was performed with 5 µg/mL FITC-conjugated Cholera toxin B subunit (Sigma Aldrich) in Hoechst (1:1000, Sigma Aldrich) for 1 hour. All pictures were taken with an Axio Observer Z1 microscope equipped with an apotome device (Zeiss, Jena, Germany). For the stainings of aged (40 weeks old) hearts and skeletal muscle (M. quadriceps femoris), these organs were harvested from C57BL/6J and *FAAH*$^{-/-}$ mice and fixated with 4% paraformaldehyde for 1 hour. Then, muscle tissues were incubated in 20% (w/v) sucrose in DPBS at 4 °C overnight and frozen in TissueTek OCT Compound (Sciences Services, Munich, Germany). Cryosections (10 µm) were permeabilized with 0.2% TritonX-100 in DPBS for 10 minutes, washed, and stained with rhodamine-labeled *Griffonia simplicifolia* lectin I (5 µg/mL, Vector Peterborough, United Kingdom) for 1 hour. Capillaries were counted automatically with the analysis module of ZEN software (Zeiss).

Real-Time-Polymerase Chain Reaction

Real-time polymerase chain reaction was exerted as described before.[26] RNA was extracted with the TRIzol reagent (Life technologies). For reverse transcription, the SuperScript VILO cDNA Synthesis Kit (Life Technologies) was used. Expression of murine FAAH and glycerinaldehyde-3-phosphate-dehydrogenase (GAPDH) was analyzed via real-time polymerase chain reaction using the following primers (Invitrogen, Karlsruhe, Germany): 5′- CTC TGG GTT TAG GAC CTG AC-3′ (*FAAH* forward) and 5′-GAG TGG GAC TGG TGT AGT TG-3′ (*FAAH* reverse), 5′- GTG TTC CTA CCC CCA ATG TG -3′ (*GAPDH* forward), and 5′- CTT GCT CAG TGT CCT TGC TG -3′ (*GAPDH* reverse). Polymerase chain reaction products were separated by 2% agarose gel electrophoresis with ethidium bromide to visualize DNA bands. Size of fragments (FAAH: 380 bp, GAPDH: 349 bp) was confirmed by the DNA marker GeneRuler DNA ladder mix (Thermo Scientific, Dreieich, Germany).

Western Blot

Western Blot analysis was performed as reported before.[27] Mouse organs, such as lung, brain, and heart, were harvested and ECs were scraped in RIPA buffer containing Complete Protease Inhibitor (Merck, Darmstadt, Germany). Mouse tissue was homogenized by a tissue lyser (Qiagen. Hilden, Germany) at 50 Hz for 8 minutes. After centrifugation at 13 000*g* for 10 minutes at 4 °C, the protein concentration of the supernatant was determined using the Bradford reagent (Sigma Aldrich). Samples were used for SDS-PAGE on a 10% (v/v) acrylamide gel. Proteins were transferred to a nitrocellulose membrane (Whatman Protran, Sigma Aldrich). The membrane was blocked for 30 minutes with 5% low-fat dry milk powder in TBST buffer containing 150 mmol/L sodium chloride, 50 mmol/L Tris-HCl, 0.05% Tween20, and incubated with primary antibody overnight at 4 °C. Following primary antibodies were used: anti-FAAH (rabbit, 1:500; Cayman Chemicals), peroxidase-coupled anti–β-actin (mouse, 1:20 000; Sigma Aldrich), peroxidase-coupled anti-GAPDH (mouse, 1:10 000; Sigma Aldrich). As secondary antibody, a peroxidase-coupled anti-rabbit antibody (1:10 000; Jackson ImmunoResearch) or anti-mouse antibody (1:10 000; Jackson ImmunoResearch) was applied for 1 hour at room temperature in TBST buffer. Western Blots were analyzed using an enhanced chemiluminescence substrate (Thermo Scientific).

MicroArray/Gene Set Enrichment Analysis

Before the microarray analysis, HUVEC were seeded in a 6-well cell culture plate (200 000 cells/well) and treated with URB (20 µmol/L), AEA (10 µmol/L), or ethanol 1 day after seeding. Twenty-four hours later, cells were lysed in 350 µL RLT lysis buffer per well (Qiagen, Hilden, Germany) and frozen at −80 °C for at least 5 minutes. For total RNA extraction lysates were thawed at room temperature, mixed with 350 µL 70% (v/v) ethanol, and further processed with Zymo Spin II columns (Zymo Research, Irvine). The column was washed with 700 µL RW1 buffer (Qiagen, Hilden, Germany) and 350 µL Zymo RNA wash buffer (Zymo Research, Irvine). Afterward, RNA was eluted in H_2O. For expression analysis, the HumanHT-12 v4 Expression Bead Chip (Illumina, San Diego) was used. On the raw microarray data background correction, log2 transformation, and quantile normalization were performed. After preprocessing, differentially expressed genes (FDR-adjusted $P<0.05$, absolute log2 fold change >1) were identified using limma package.[28] To obtain a functional overview of enriched biological processes and signaling pathways, gene set enrichment analyses were performed on c2 and c5 gene set databases downloaded from MSigDB[29] using R package HTSanalyzeR.[30] All bioinformatics analyses were performed using R 3.2.3.

Transcription Factor Analysis

For TF (transcription factor) analysis the potential binding sites for TFs were detected at the promoters (upstream 1 kb and downstream 100 bp of transcription start site) of all differentially expressed genes using FIMO with default parameters ($P<1\times10^{-4}$), based on position frequency matrices from JASPAR database (http://jaspar.genereg.net/). To identify the potential pathways associated with the target genes of each TF, we performed functional annotation using hypergeometric tests (FDR-adjusted $P<0.05$) based on Kyoto Encyclopedia of Genes and Genomes databases.

Analysis of Choroidal Neovascularization In Vivo

C57BL/6J wild-type mice (Bl6, Janvier, Le Genest St. Isle, France) and *FAAH*$^{-/-}$ mice (kindly provided by Professor Dr Zimmer, Institute of Molecular Psychiatry, University of Bonn, Germany) were used. Animals were anesthetized by intraperitoneal injection of 60 mg ketamine/kg body weight and 5 mg xylazine/kg body weight. Pupils were dilated by topic application of eye drops containing 0.5% (w/v) tropicamide (Mydriaticum Stulln, Pharma Stulln, Stulln, Germany) and 10% (w/v) phenylephrine. Four to 5 laser lesions surrounding the optic nerve head were created under the following conditions: excitation: 514 nm, pulse duration: 0.1 s, laser power: 200 mW, spot size: 50 µm. Reflectance imaging and fluorescein angiography were performed 14 days following the laser treatment by confocal scanning laser ophthalmoscopy (HRA2, Heidelberg Engineering, Heidelberg, Germany). Therefore, a 10% (w/v) fluorescein solution (Alcon Pharma, Freiburg, Germany) was injected intraperitoneally at a concentration of 50 mg fluorescein/kg body weight. Images were taken before injection, 3 to 4 minutes (early phase), and 6 to 8 minutes (late phase) after dye injection with different focus settings (+10 d to +30 d). To prevent cataract formation and to optimize image clarity, lubricating eye drops (oculotect

fluid, Novartis Pharma, Nuernberg, Germany) were applied to the eyes every 1 to 2 minutes. In vivo imaging was followed by topical administration of Corneregel (Bausch&Lomb, Berlin, Germany).[31] Fluorescence angiograms (late phase) from day 14 were chosen to determine pixel intensity and the neovascular area of the laser lesions. Furthermore, 2 blinded persons graded the lesions (early and late phase) according to the following classification: 0=no leakage, 1=questionable leakage, hyperfluorescence without increase in intensity or size; 2a=leakage, hyperfluorescence with increase in intensity but not in size; 2b=pathologically significant leakage, hyperfluorescence with increase in intensity and size.[32]

Preparation and Staining of Choroidal Flatmounts

Mice were killed on day 24 following laser treatment using 100% carbonic gas and immediately enucleated. The whole eye was dissected and fixated with 4% (w/v) paraformaldehyde overnight. For histological staining, the fixed eyes were dehydrated, embedded in paraffin, sliced (5 µm), and stained with hematoxylin and eosin as described elsewhere.[33] Pictures were taken with an Axiovert 200 M microscope (Zeiss, Jena, Germany). For fluorescence staining, fixed eyes were washed with DPBS, the choroid was separated from the retina, and permeabilized with 2% (v/v) TritonX-100 for 20 minutes. Staining with rhodamine-labeled *Griffonia simplicifolia* lectin I (1:100, Vector Peterborough, United Kingdom) was performed for 1 hour, and pictures were taken with an Axio Observer Z1 microscope including an apotome device (Zeiss).

Statistical Analysis

Data are expressed at mean±SEM. Normality and variance were not tested to determine whether the applied parametric tests were appropriate. Statistical significance was determined by 1-way ANOVA with Tukey post hoc test, unpaired 2-tailed Student *t* test, or χ^2 test using GraphPad Prism 5 (Graphpad Software, Inc). Results were considered significant if P was <0.05, $^{*}P<0.05$, $^{**}P<0.01$, $^{***}P<0.001$.

Animal Experiments

Animal housing and experiments were performed corresponding to the guidelines of the German law of protection of animal life with permission by the local government authorities (Landesamt für Natur, Umwelt und Verbraucherschutz Nordrhein-Westfalen, NRW, Germany) and complied with the Association for Research in Vision and Ophthalmology Statement for the Use of Animals in Ophthalmic and Vision Research. For ex vivo and in vivo experiments, female C57BL/6J and *FAAH*$^{-/-}$ mice at an age of >4 weeks were applied. Female mice were used because age-related macular degeneration is more prevalent in women.

RESULTS

FAAH Inactivation Reduces Vascular Sprouting In Vitro and Ex Vivo

To test the potential involvement and function of the FAAH enzyme for vascular growth, we first examined mRNA expression of FAAH in human ECs and found FAAH expression in HUVEC as well as human microvascular ECs derived from lung. Expression levels were comparable to those of other cell types, that is, human lung fibroblasts (Figure IA in the Data Supplement). More importantly, protein expression of FAAH was detected using Western Blot analysis in several EC lines, such as HUVEC, human microvascular ECs derived from lung and bovine pulmonary arterial ECs (Figure IB in the Data Supplement). As positive and negative controls for FAAH expression, we used mouse lung, brain, and heart, respectively (Figure IC in the Data Supplement). These findings were also supported by immunohistochemistry revealing prominent FAAH expression in single HUVEC (Figure ID in the Data Supplement), human microvascular ECs derived from lung (Figure IE in the Data Supplement) as well as bovine pulmonary artery EC (Figure IF in the Data Supplement).

Next, we tested whether FAAH inhibition had an effect on angiogenesis using 2 types of cell culture models: HUVEC, as an established and well-characterized cell line, that is frequently applied for angiogenesis assays, and transgenic *flt1/eGFP* ES cells (*flt1/eGFP* ES cells),[18] that express the reporter gene eGFP under control of the *flt1* promoter. This transgenic cell line displays EC–specific eGFP expression in the developing vasculature. Vascularization during ES cell differentiation resembles a more physiological model for in vitro angiogenesis, as the sprouts grow in a 3-dimensional matrix of different cell types, similar as found within the body. To investigate the effect of FAAH inhibition on angiogenesis, HUVEC were treated for 24 hours with different concentrations of the pharmacological FAAH inhibitor URB597 (10–100 µmol/L). In the matrigel-based angiogenesis assay, URB597 dose-dependently (starting at 20 µmol/L) decreased vascular tube length (Figure 1A, 1B, 1E), the amount of branching points (Figure 1A, 1B, and 1G), and vascular loops (Figure 1A and 1B, Figure IIA in the Data Supplement). Although native HUVEC formed vascular networks with a tube length of 4.9±0.3 mm/mm^2, 10.1±1.0 branching points/mm^2 and 6.5±0.6 vessel loops/mm^2, n=9 (Figure 1A, 1E, and 1G, Figure IIA in the Data Supplement), treatment of the cells with URB597 (20 µmol/L) decreased tube length to 2.9±0.3 mm/mm^2 (n=4, $P<0.01$), branching points to 4.6±0.4 /mm^2 (n=4, $P<0.05$), and vessel loops to 3.0±0.4 /mm^2 (n=4, $P<0.01$) (Figure 1B, 1E, and 1G, Figure IIA in the Data Supplement). Also anandamide (AEA, 10 µmol/L), the substrate of FAAH, and methanandamide (Met-AEA, 5 µmol/L), a nonhydrolyzable AEA analog, strongly reduced tube length (Figure 1C, 1D, and 1F), the number of branching points (Figure 1C, 1D, and 1H), and vascular loops (Figure 1C and 1D, Figure IIB in the Data Supplement) compared with controls. Importantly, the solvents alone did not affect vascular growth parameters (Figure 1E through 1H, Figure

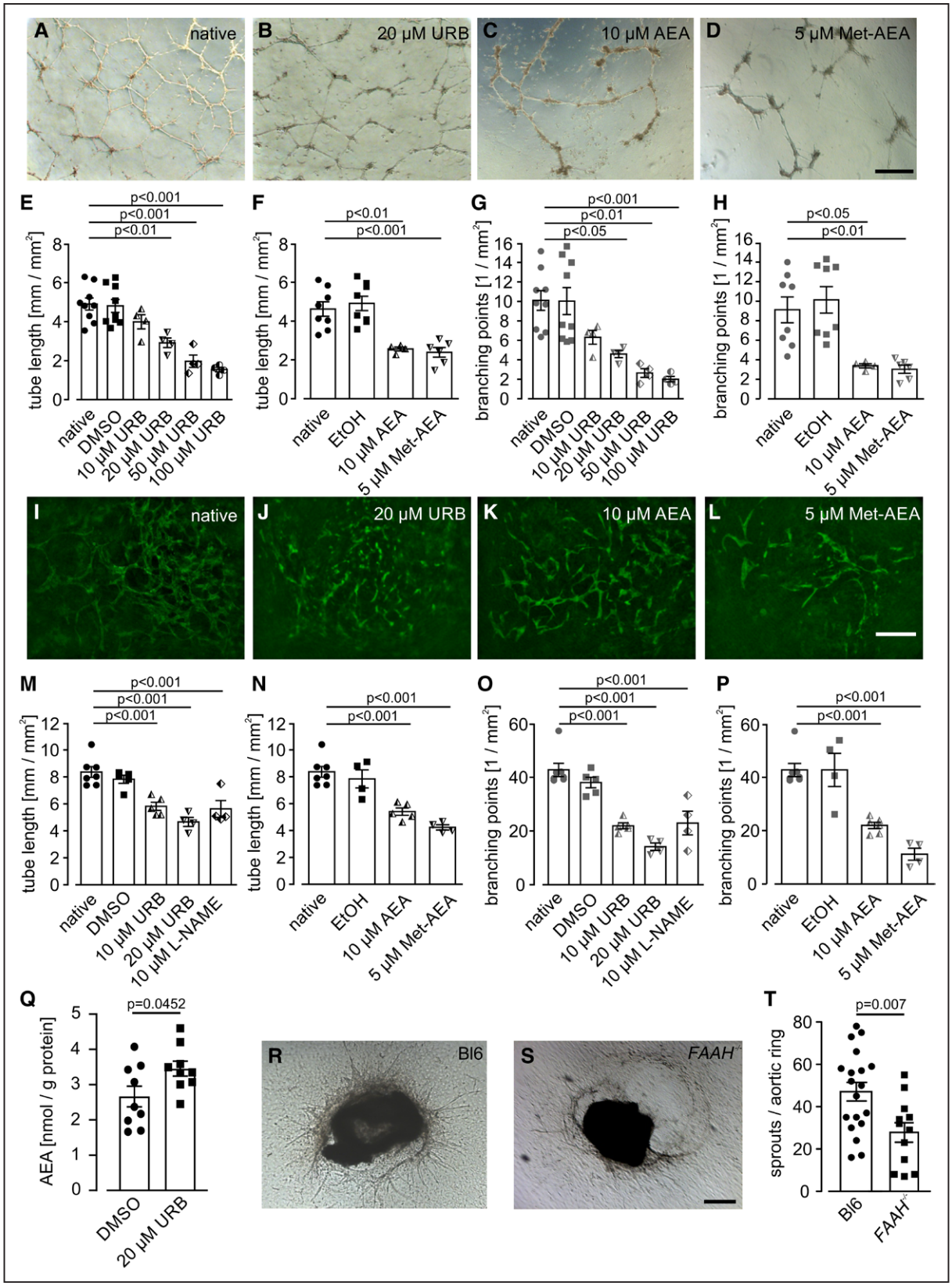

Figure 1. Inhibition or lack of FAAH (fatty acid amide hydrolase) impairs angiogenesis of human umbilical vein endothelial cell (HUVEC) and embryonic stem cell (ESC)–derived EC in vitro and in an aortic ring assay ex vivo.

A–**D**, Phase-contrast images of endothelial network formation in matrigel of native HUVEC (**A**) and HUVEC treated with 20 µmol/L URB597 (URB) (**B**), 10 µmol/L anandamide (AEA; **C**), or 5 µmol/L methanandamide (Met-AEA; **C**); bar=500 µm. **E**–**H**, Quantification of HUVEC network formation in matrigel: tube length (**E** and **F**), branching points (**G** and **H**) (n=4–9); (*Continued*)

IIA and IIB in the Data Supplement). Similar results as with HUVEC were also observed in the angiogenesis assay of differentiating *flt1/eGFP* ES cells. In this assay 10 µmol/L of URB597 reduced tube length (Figure 1I, 1J, and 1M), branching points (Figure 1I, 1J, and 1O) and vascular loops (Figure 1I and 1J, Figure IIC in the Data Supplement) to a similar degree as the well-established angiogenesis inhibitor N-nitro-L-arginine methyl ester hydrochloride (10 µmol/L). Incubation with AEA (10 µmol/L) or Met-AEA (5 µmol/L) caused a comparable reduction of vascular network formation as FAAH inhibition by URB597 (10 µmol/L), whereas there was again no effect of the solvents (Figure 1M through 1*P*, Figure IIC and IID in the Data Supplement). These data suggest that FAAH inhibition and elevated AEA levels impair angiogenesis in vitro via a direct action of AEA. To demonstrate that ECs produce AEA and to confirm that URB597-treatment enhances AEA levels, we exposed HUVEC to the pharmacological FAAH inhibitor URB597 (20 µmol/L) or the solvent DMSO in serum-free medium for 24 hours and determined AEA concentrations in cell homogenates by liquid chromatography-multiple reaction monitoring. As expected, we found elevated AEA levels in response to URB597 (URB597: 3.5±0.2 nmol/g (n=9), DMSO: 2.7±0.3 nmol/g (n=9), P=0.0452, Figure 1Q). These data further confirm that the observed effects of URB597 on AEA levels are due to its inhibition of FAAH.

To exclude potential unspecific actions of the pharmacological FAAH inhibitor and to test the effect of genetic FAAH inhibition on angiogenesis ex vivo, next we examined vascular sprouting in an aortic ring assay comparing C57BL/6J control and *FAAH*$^{-/-}$ mice (Figure 1R through 1T). Aortic rings were transferred to a collagen gel and sprouting was quantified on day 8. The average number of sprouts/ring in C57BL/6J aortas was 47.1±4.8, n=19 (Figure 1R and 1T), whereas in *FAAH*$^{-/-}$ mice, it was significantly reduced to 29.5±3.5 sprouts/ring, n=18 (Figure 1S and 1T), P=0.007. This finding revealed that genetic FAAH deficiency results in reduced angiogenesis further confirming the above-reported effects of pharmacological inhibition of FAAH on vessel formation.

FAAH Inhibition Downregulates Genes Involved in Cell Cycle Progression and DNA Replication

To obtain further insight into the effects of FAAH inhibition on angiogenesis a microarray of untreated, ethanol-treated (solvent), URB597-treated (20 µmol/L), and AEA-treated (10 µmol/L) HUVEC (n=3) was performed. In full agreement with the angiogenesis assays changes of gene regulation induced by URB597 and AEA were quite similar (Figure 2A, Pearson correlation coefficient=0.57, $P<1\times10^{-6}$). Top 25 up and downregulated genes in response to URB597 or AEA treatment can be found in Tables I and II in the Data Supplement and are displayed in Figure III in the Data Supplement.

Then, gene set enrichment analysis was performed using HTSanalyzeR[30] for identification of altered biological processes in response to URB597 and AEA treatment: Out of the total 6179 gene sets (c2: curated gene sets and c5: gene ontology gene sets) obtained from MSigDB,[29] 1335 and 1686 gene sets were found to be significantly affected by URB597 and AEA treatment, respectively (Benjamini-Hochberg adjusted P<0.001). Importantly, 950 gene sets were significantly enriched in both URB597-treated and AEA-treated HUVEC, suggesting functional overlap (Figure 2B, $P<1\times10^{-6}$, hypergeometric test). More specifically, both compounds downregulated genes involved in cell cycle progression (n=3, URB, AEA versus native P<0.001) (Figure 2C and 2D) and DNA replication (n=3, URB, AEA versus native P<0.001) (Figure 2E and 2F). Additionally, genes contributing to integrin binding (n=3, URB versus native P<0.05, AEA versus native P<0.01) (Figure 2G and 2H) and tissue development (n=3, URB, AEA versus native P<0.05) (Figure 2I and 2J) were downregulated in response to URB597 and AEA incubation. No genes were identified to be differentially expressed between ethanol and native conditions, confirming that the solvent alone has no effect. Thus, gene set enrichment analysis suggests the reduction of cell cycle activity by both FAAH inhibition and AEA treatment; it also points towards a negative impact of these interventions on integrin binding and tissue development. To get further insights into the role of FAAH inhibition in integrin signaling, we then analyzed this gene set in detail and found that genes of several integrin-binding proteins modulating cell adhesion or angiogenesis were downregulated (VWF [von Willebrand factor], ADAM9/23 [disintegrin and metalloproteinase 9/23], ICAM2 [intercellular cell adhesion molecule 2])[34–37] (Figure 2K).

In addition, we also performed TF analysis to identify TFs that may contribute to the differential transcriptome after URB597 and AEA treatment. First, 15 differentially expressed TFs after URB597 treatment (Figure IVA in the Data Supplement) and 3 differentially

Figure 1 Continued. (**I**–**L**) fluorescence images of endothelial network formation of native flt1 (fms-like tyrosine kinase 1)/eGFP (enhanced green fluorescence protein) ESC (**I**) or *flt1/eGFP* ESC treated with 20 µmol/L URB (**J**), 10 µmol/L AEA (**K**) or 5 µmol/L Met-AEA (**L**); bar=100 µm. **M**–**P**, Quantification of endothelial network formation of *flt1/eGFP* ESC: tube length (**M** and **N**), branching points (**O** and **P**) (n=4–7). Same values for native were used for (**M**) and (**N**) as well as for (**O**) and (**P**). **Q**, Quantification of AEA in HUVEC in response to URB (20 µmol/L). **R** and **S**, Phase-contrast images of aortic ring assay using aortas of C56BL/6J (Bl6) (**R**) and *FAAH*$^{-/-}$ (**S**) mice; bar=400 µm. **T**, Quantification of sprouts in aortic ring assay (N=7, n=12–19). **E**–**H** and **M**–**P**, One-way ANOVA, Tukey post hoc test; (**Q** and **T**) 2-tailed unpaired *t* test. DMSO indicates dimethyl sulfoxide; EtOH, ethanol; and L-NAME, N-nitro-L-arginine methyl ester hydrochloride.

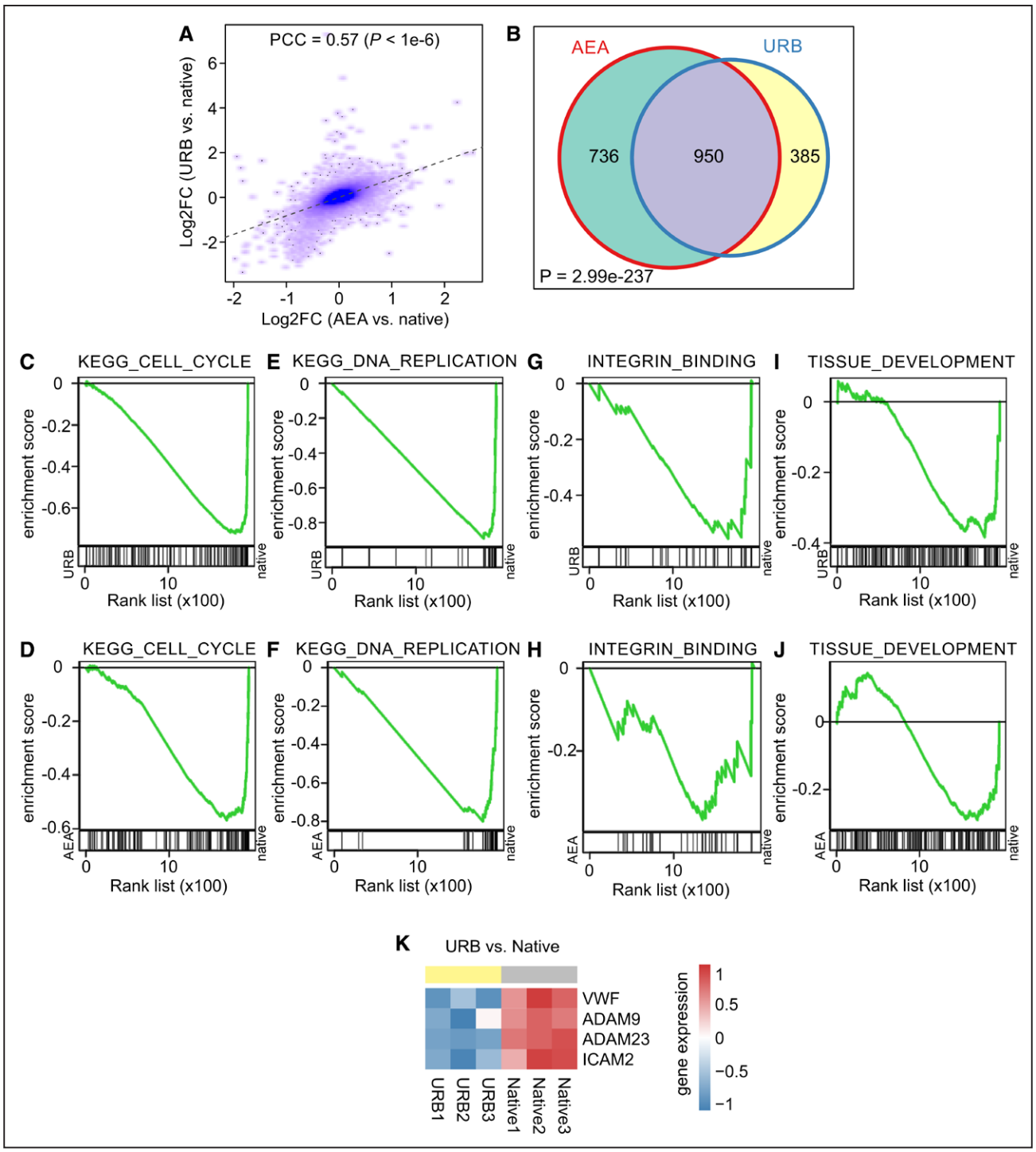

Figure 2. FAAH (fatty acid amide hydrolase) inhibition in endothelial cells (ECs) reduces expression of genes for cell cycle progression, integrin binding, and tissue development.

A, Correlation analysis of gene expression changes (Pearson correlation coefficient=0.57, $P<1\times10^{-6}$). **B**, Venn diagram of gene sets enriched in URB597 (URB)- and anandamide (AEA)-treated human umbilical vein EC (HUVEC; hypergeometric test, $P<1\times10^{-6}$). **C**–**J**, Gene set enrichment analysis score curves. For gene set enrichment analysis, HUVEC treated with 20 µmol/L URB (n=3) (**C**, **E**, **G**, and **I**) or 10 µmol/L AEA (n=3) (**D**, **F**, **H**, and **J**) were compared with native cells (n=3). The following gene clusters are displayed: Kyoto Encyclopedia of Genes and Genomes (KEGG)_Cell_Cycle (**C**+**D**), KEGG_DNA_Replication (**E**+**F**), Integrin_Binding (**G**+**H**), Tissue_Development (**I**+**J**). **K**, Heatmap of differentially expressed genes related to integrin binding. ADAM indicates disintegrin and metalloproteinase; ICAM, intercellular cell adhesion molecule; and VWF, von Willebrand factor.

expressed TFs after AEA treatment (Figure IVB in the Data Supplement) were found. Next, we analyzed the potential binding sites for 746 TFs at the promoters of all differentially expressed genes and identified 8 differentially expressed TFs that bind to a promoter region of these genes after URB597 treatment

(Figure IVC in the Data Supplement); we also detected 2 differentially expressed TFs that bind to a promoter region of differentially expressed genes after AEA treatment (Figure IVD in the Data Supplement). Next, based on 8 overlapping TFs and 351 target genes that are differentially expressed after URB597 treatment, we have generated a TF regulatory network (Figure V in the Data Supplement). To identify the potential pathways associated with the target genes of each TF, we performed functional annotation using hypergeometric tests (FDR-adjusted $P<0.05$) based on Kyoto Encyclopedia of Genes and Genomes database.[38] We found that KLF4 and EGR1 target genes are associated with p53 signaling pathway, cellular senescence, Fanconi anemia pathway, cell cycle, and DNA replication; BCL6B target genes are associated with Fanconi anemia pathway; MSX1 are associated with DNA replication; E2F2 target genes are associated with cell cycle and DNA replication (Figure VI in the Data Supplement).

Inhibition of FAAH Reduces EC Proliferation and Migration and Induces Cell Cycle Exit

Gene expression analysis provided some hints for the signaling mechanisms underlying the antiangiogenic effects of FAAH inhibition and AEA application. Therefore, we then performed cell biological experiments to test the effects on EC behavior.

First, the impact of URB597 and AEA on proliferation was examined using Ki67 staining of HUVEC (Figure 3A through 3D). The analysis revealed that in untreated HUVEC 42.3±2.1% (n=10) of all Hoechst$^+$ nuclei also displayed Ki67$^+$ staining, whereas treatment with URB597 or AEA strongly reduced Ki67$^+$/Hoechst$^+$ cells to 20.7±6.3% (n=4, $P<0.01$) or 23.1±5.2% (n=4, $P<0.01$), respectively; the solvents had no effect on Ki67 expression (Figure 3D).

To test if FAAH inhibition specifically affects cell growth of EC but not of other cell types, we exposed human aortic smooth muscle cells to 20 µmol/L URB597 for 24 hours. Then, Ki67 staining was performed and Ki67$^+$Hoechst$^+$ cells were quantified. The analysis revealed that in contrast to HUVEC URB597 did not affect the fraction of Ki67$^+$Hoechst$^+$ human aortic smooth muscle cells when compared with native cells and DMSO solvent controls (Figure VIIA in the Data Supplement).

To further corroborate that the URB597 effect in EC is mediated by AEA and not by other endocannabinoid-like compounds hydrolyzed by FAAH or being the product of such hydrolysis, we tested arachidonic acid (10 µmol/L), oleoylethanolamide (10 µmol/L), and palmitoylethanolamide (10 µmol/L). None of these compounds affected the number of Ki67$^+$/Hoechst$^+$ HUVEC, whereas the positive control Met-AEA (5 µmol/L) strongly reduced the number of cells in the cell cycle (Figure VIIB in the Data Supplement). Thus, URB597-induced inhibition of cell growth selectively affects EC, and this effect is mediated by AEA. To further prove that URB597 affects EC growth via FAAH inhibition, we performed a knockdown of FAAH using RNAi by treating HUVEC with a lentiviral FAAH shRNA construct and counted Ki67$^+$/Hoechst$^+$ cells. We found that lentiviral knockdown of FAAH reduced the number of Ki67$^+$ HUVEC to the same extent as 20 µmol/L of the FAAH inhibitor URB597. Interestingly, additional application of URB597 after FAAH knockdown did not further decrease the number of Ki67$^+$ HUVEC confirming the specificity of the inhibitory action of URB597 on FAAH (Figure VIIC in the Data Supplement). We also explored the dose-dependency of the effect by applying Met-AEA. The observed left shift in response to URB597 underscored that the effect of FAAH inhibition is mediated by AEA signaling and not due to unspecific toxic effects of high AEA concentrations (Figure VIID in the Data Supplement).

In a next step, we examined the effect of FAAH inhibition on proliferation and migration of EC by a scratch assay (Figure 3E through 3H). After 8 hours, untreated cells covered 51.1±6.0% (n=4) of the scratch area, whereas URB597 decreased the covered area to 16.9±2.8% (n=4, $P<0.001$) and AEA limited regrowth of the cells to 31.8±4.7% (n=5, $P<0.05$) of the scratch area (Figure 3E through 3H). To test if FAAH inhibition can also cause apoptosis, HUVEC were stained with fluorescein-conjugated AnnexinV (AnnexinV-FITC) as well as propidium iodide and analyzed via flow cytometry (Figure 3I through 3L). We found that untreated as well as URB597-treated or AEA-treated HUVEC only displayed low numbers of FITC$^+$propidium iodide$^+$ apoptotic cells (3.4±0.4%, n=4 [native, Figure 3I and 3L], 3.3±0.6%, n=4 [URB597, Figure 3J and 3L], 2.6±0.9%, n=4 [AEA, Figure 3K and 3L]). As a positive control, HUVEC were incubated without serum for 24 hours and showed much higher numbers of apoptotic cells (11.1±0.2%, n=4; $P<0.001$) (Figure 3L). Thus, inhibition of FAAH reduces proliferation and migration of HUVEC but has no effect on apoptosis. These results confirm that FAAH inhibition modulates the cell cycle. To investigate this more in detail, we performed cell cycle analysis using propidium iodide staining and flow cytometry (Figure 3M and 3N, Figure VIII in the Data Supplement). URB597 treatment increased the number of EC in G0/G1 stage from 70.2±1.5%, n=4 (native) to 80.9±1.1%, n=4, $P<0.001$ (URB597), whereas it decreased the amount of EC in S phase from 16.0±0.7%, n=4 (native) to 11.0±0.9%, n=4, $P<0.01$ (URB597); the solvent had no effect (Figure 3M). Treatment with AEA showed similar effects, as it increased the number of cells in G0/G1 stage from 69.1±1.2%, n=8 (native) to 77.3±2.7%, n=5, $P<0.05$

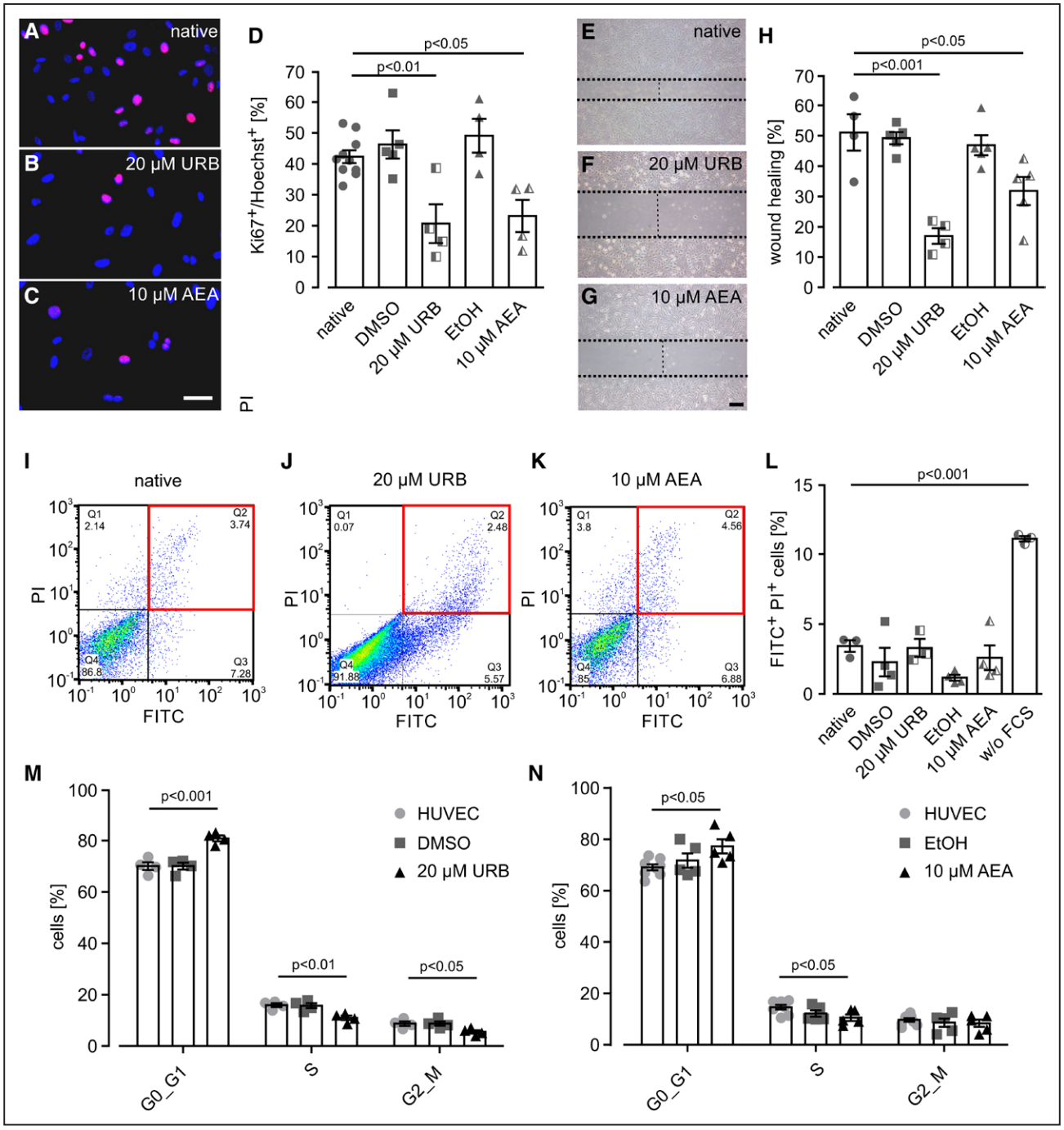

Figure 3. URB597 (URB) reduces proliferation, migration, and cell cycle activity in human umbilical vein endothelial cells (HUVEC).

A–**C**, Immunofluorescence staining of native HUVEC (**A**) or HUVEC treated with 20 µmol/L URB (**B**) or 10 µmol/L anandamide (AEA; **C**); red=Ki67, blue=Hoechst, bar=50 µm. **D**, Quantification of the number of proliferating Ki67$^+$ cells (n=4–10). **E**–**G**, Phase-contrast images of a scratch assay with native HUVEC (**E**) or HUVEC treated with 20 µmol/L URB (**F**) or 10 µmol/L AEA (**G**); bar=400 µm. **H**, Quantification of wound healing in scratch assay (n=4–5). **I**–**K**, Flow cytometry analysis of HUVEC stained with AnnexinV–fluorescein isothiocyanate (FITC) and propidium iodide (PI): native HUVEC (**I**), HUVEC treated with 20 µmol/L URB (**J**), or 10 µmol/L AEA (**K**). **L**, Quantification of apoptotic cells (FITC$^+$ PI$^+$) (n=3–4). **M** and **N**, Quantification of cell cycle analysis by PI staining and flow cytometry (n=4–8). **D**, **H**, **L**, **M**, and **N**, 1-way ANOVA, Tukey post hoc test. DMSO indicates dimethyl sulfoxide; EtOH, ethanol; and w/o, without.

(AEA), whereas the number of cells in S phase was reduced from 14.7±0.9%, n=8 (native) to 10.5±1.2%, n=5, $P<0.05$ (AEA) (Figure 3N). These data demonstrate that, as suggested by gene expression analysis, FAAH inhibition results in cell cycle exit of EC. This as well as the reduced proliferation and migration of EC underlie impaired angiogenesis upon FAAH inhibition in in vitro and ex vivo assays.

FAAH Inhibition Results in Disintegration of Lipid Rafts and Has Similar Effects on Angiogenesis as the Lipid Raft Disruptor MβC

To further explore the signaling mechanism underlying reduced angiogenesis upon FAAH inhibition, we tested whether URB597-dependent inhibition of EC proliferation could be prevented by blocking well-known cannabinoid receptors or related enzymes. This was not the case, as neither application of SR141716 (1 µmol/L, CB1 [cannabinoid receptor 1] receptor antagonist), SR144528 (1 µmol/L, CB2 receptor antagonist), O-1918 (1 µmol/L, endothelial non-CB1/CB2 receptor antagonist), indomethacin (1 µmol/L) nor capsazepine (1 µmol/L, TRPV1 [transient receptor potential cation channels of the vanilloid type] antagonist) affected the number of Ki67$^+$ EC treated with URB597 (Figure IX in the Data Supplement). These findings suggest that none of the canonical cannabinoid pathways is involved.

Because endocannabinoid effects that are independent from cannabinoid receptors have previously been attributed to lipid rafts,[39] we have performed immunostainings of lipid rafts with FITC-labeled Cholera toxin B in HUVEC. The cells were treated with URB597 (20 µmol/L), AEA (10 µmol/L), or the lipid raft disruptor MβC (10 mmol/L) (Figure 4A through 4E). Our experiments revealed that the FAAH inhibitor URB597 (Figure 4C) and AEA (Figure 4D) induced a similar effect as MβC (Figure 4E) in regard to disintegration of lipid rafts, whereas solvent controls were unaffected (Figure 4A and 4B). To exclude that other mediators than AEA are responsible for lipid raft disturbance, we treated HUVEC with arachidonic acid, oeloylethanolamide, and palmitoylethanolamide. None of these could affect the structure of lipid rafts, whereas Met-AEA used as a positive control did induce similar changes as URB and AEA (Figure XA through XF in the Data Supplement). Thus, the antiproliferative and antimigratory response to FAAH inhibition in EC appears to be mediated by AEA and a lipid raft-dependent process. This is underscored by the finding that treatment of EC with MβC had very similar effects on angiogenesis, proliferation, and migration as URB597 or AEA: HUVEC treated with MβC exhibited a decreased network formation in matrigel (Figure 4F through 4H). This was due to reduced tube length (Figure 4I), number of branching points (Figure 4J), and vascular loops (Figure 4K) of HUVEC after MβC treatment. In analogy to URB597 and AEA, MβC application induced a decrease of the number of Ki67$^+$ EC (Figure 4L through 4O), wound healing capacity (Figure 4P through 4S), and had no effect on apoptosis (Figure 4T through 4W). Taken together, these results imply that pharmacological FAAH inhibition disrupts lipid rafts causing an impairment of vascular growth.

FAAH Deficiency Protects Against Pathological Angiogenesis in the Choroidal Neovascularization Model In Vivo

Finally, we wanted to know if the antiangiogenic effect of FAAH deficiency can be also exploited in a disease characterized by excessive vessel growth. For that purpose, we have chosen laser-induced choroidal neovascularization (CNV) in mouse, which is a model for wet age-related macular degeneration in humans. In this model, laser photocoagulation is applied to induce a break in Bruch's membrane (Figure 5A) resulting in angiogenesis from the choriocapillaris. On day 14 after the injury, we quantified CNV by fluorescence angiography in C57BL/6J (Bl6) and *FAAH*$^{-/-}$ mice (Figure 5B through 5H). The analysis demonstrated that in the late stage of the angiogram (6–8 minutes after fluorescein injection) leakage was significantly reduced in *FAAH*$^{-/-}$ animals (pixel intensity: 99.6±11.8, n=6) (Figure 5E and 5F) compared with Bl6 mice (pixel intensity: 160.3±14.9, n=7, P=0.002) (Figure 5C and 5F); the same was found for the size of the neovascularized area (28340±6864 pixels, n=7 [*FAAH*$^{-/-}$] versus 48470±6818 pixels, n=6 [C57BL/6J], P=0.043) (Figure 5G). Furthermore, grading of the lesions revealed a clearly decreased number of more severe grade 2b lesions (strong leakage, increasing in area and size) in *FAAH*$^{-/-}$ mice (15.3%, n=7 [*FAAH*$^{-/-}$]) compared with controls (41.7%, n=6 [Bl6], P<0.05) (Figure 5H). Then, the neovascular area was quantified in lectin-stained choroidal flatmounts at day 24 after laser treatment (Figure 5I through 5L). Also, these analyses confirmed a clearly reduced neovascular area in *FAAH*$^{-/-}$ mice (Figure 5K and 5L) compared with Bl6 controls (Figure 5I, 5J, and 5L) (19210±2767 µm^2, n=7 [*FAAH*$^{-/-}$] versus 29380±4112 µm^2, n=6 [Bl6], P<0.05). Thus, FAAH deficiency results in a prominent reduction of pathological angiogenesis in the laser-induced mouse model of CNV in vivo. To exclude that FAAH deficiency compromises physiological vascular remodeling in older individuals, we compared the number of lectin-stained capillaries in heart and skeletal muscle of Bl6 and *FAAH*$^{-/-}$ mice (40 weeks old). Our analysis demonstrated that there were no differences in the amount of capillaries in heart (2660±102.8, n=5 [Bl6] versus 2410±64.5, n=5 [*FAAH*$^{-/-}$], P>0.05) or skeletal muscle (565.8±46.9, n=5 [Bl6] versus 431.3±73.1 [*FAAH*$^{-/-}$], P>0.05) in Bl6 and *FAAH*$^{-/-}$ mice (Figure XG and XH in the Data Supplement). Therefore, FAAH targeting could be a promising approach for the treatment of pathological neovascularization, as chronic inhibition of FAAH does not appear to have deleterious effects on vascular remodeling.

DISCUSSION

In this study, we demonstrate that FAAH inhibition strongly decreases angiogenesis. The antiangiogenic effect of FAAH inhibition was also found in a highly relevant in vivo model, as *FAAH*$^{-/-}$ mice proved to be protected from choroidal neovascularization. This is due to EC cell cycle exit resulting in a reduction of EC proliferation and migration. The FAAH-related antiangiogenic response is not mediated via classic cannabinoid signaling pathways

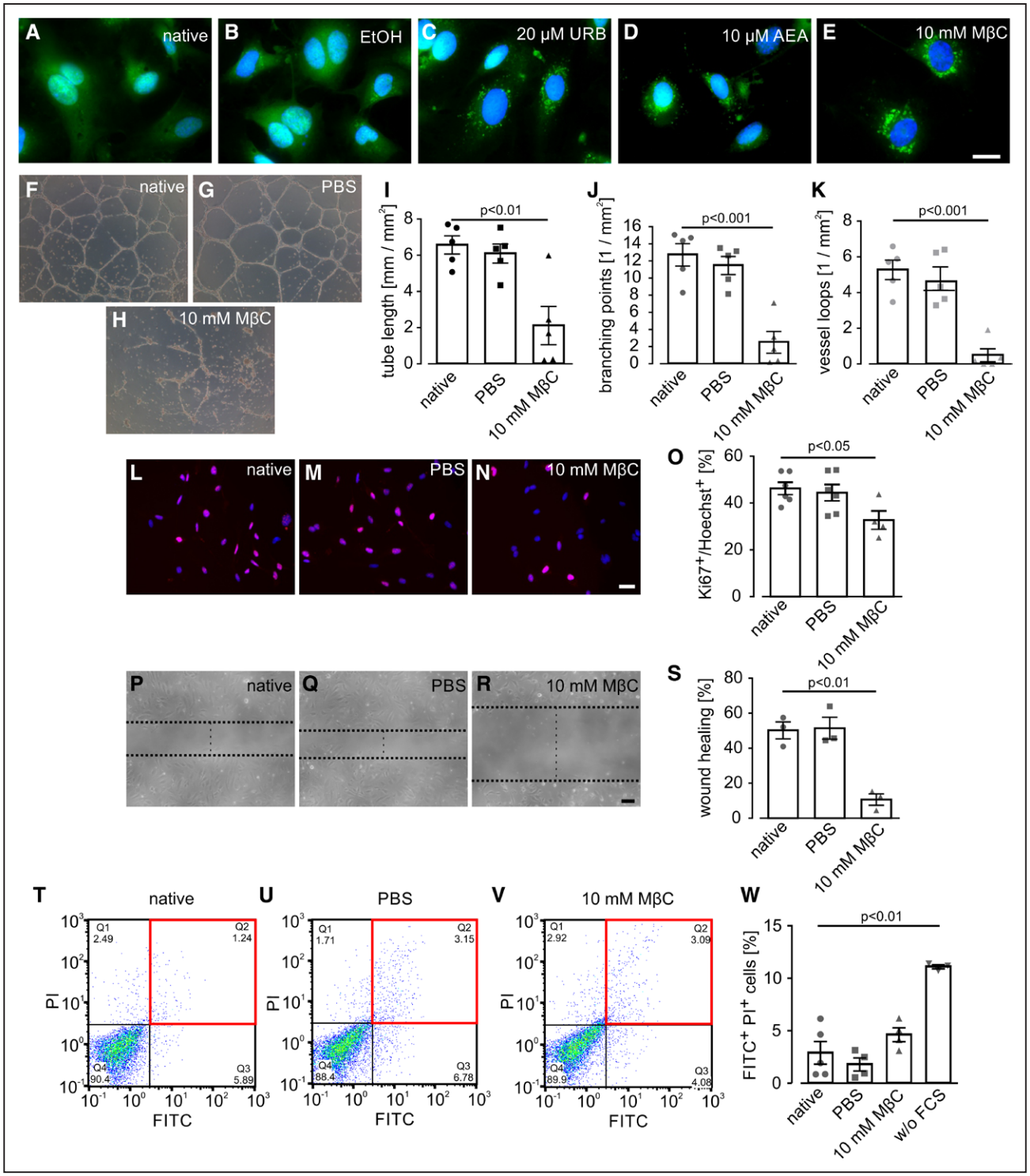

Figure 4. Depletion of cholesterol via methyl-β-cyclodextrin (MβC) inhibits angiogenesis, endothelial cell (EC) proliferation, and migration.

A–**E**, Staining of lipid rafts with fluorescein isothiocyanate (FITC)–conjugated Cholera toxin B subunit in native human umbilical vein endothelial cells (HUVEC; **A**) or HUVEC treated with ethanol (EtOH; **B**), 20 µmol/L URB597 (URB; **C**), 10 µmol/L anandamide (AEA; **D**) or 10 mmol/L MβC (**E**); bar=20 µm. **F**–**H**, Phase-contrast images of endothelial network formation in matrigel of native HUVEC (**F**) and HUVEC treated with PBS (**G**) or 10 mmol/L MβC (**H**); bar=500 µm. **I**–**K**, Quantification of HUVEC network formation in matrigel: tube length (**I**), branching points (**J**), vessel loops (**K**) (n=5). **L**–**N**, Immunofluorescence staining of native HUVEC (**L**) or HUVEC treated with PBS (**M**) or 10 mmol/L MβC (**N**); red=Ki67, blue=Hoechst, bar=50 µm. **O**, Quantification of the number of proliferating Ki67⁺ cells (n=4–6). **P**–**R**, Phase-contrast images of a scratch assay with native HUVEC (**P**) or HUVEC treated with PBS (**Q**) or 10 mmol/L MβC (**R**); bar=100 µm. **S**, Statistical analysis of wound healing in scratch assay (n=3). **T**–**V**, Flow cytometry analysis of HUVEC stained with AnnexinV-FITC and propidium iodide (PI): native HUVEC (**T**), HUVEC treated with PBS (**U**) or 10 mmol/L MβC (**V**). **W**, Quantification of apoptotic cells (FITC⁺ PI⁺) (n=3–5). **I**–**K**, **O**, **S**, and **W**, 1-way ANOVA, Tukey post hoc test.

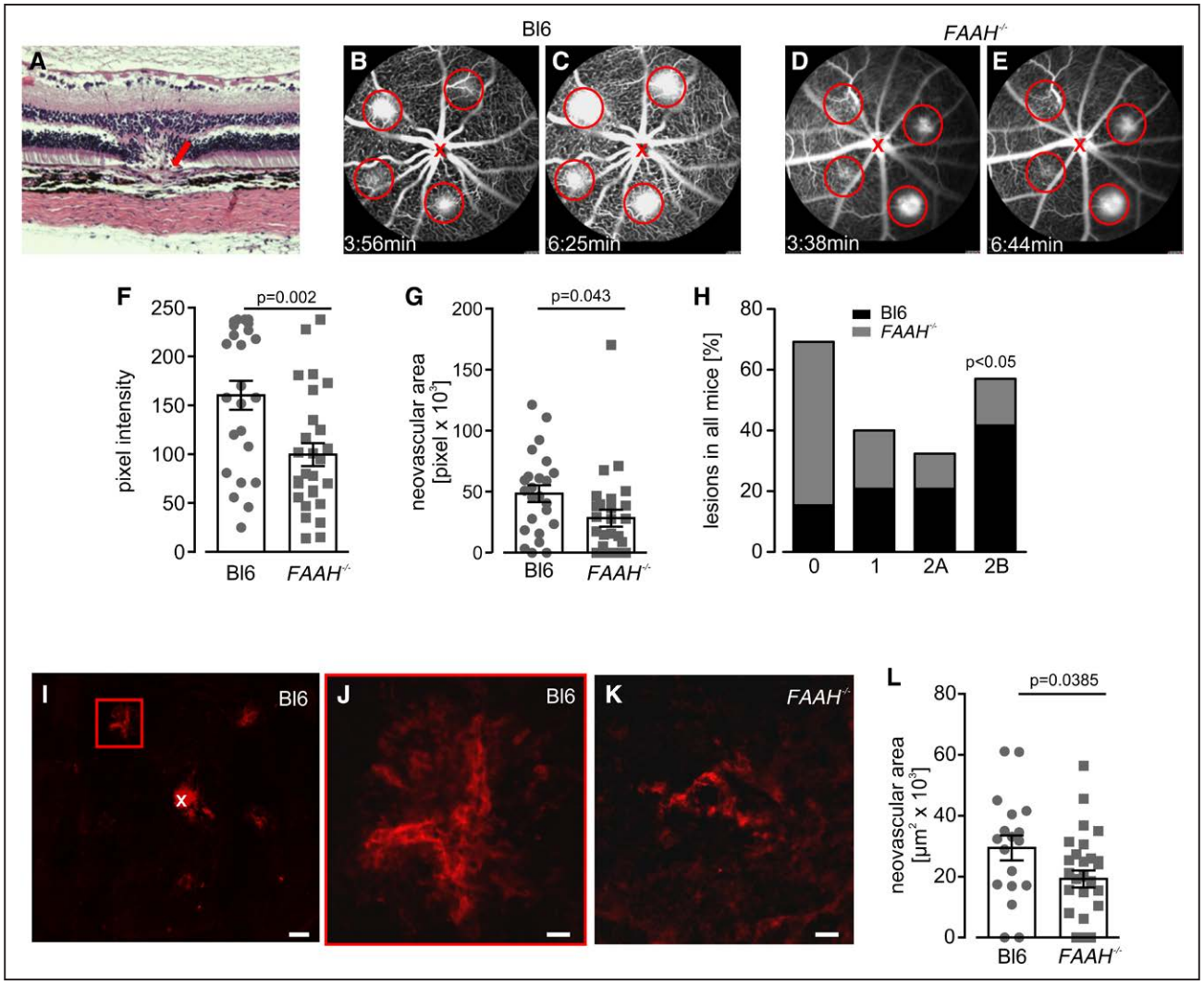

Figure 5. FAAH (fatty acid amide hydrolase) deficiency prevents choroidal neovascularization in vivo.
A, Hematoxylin and eosin staining of a C56BL/6J (Bl6) mouse retina cross-section. The arrow points towards the lesion in Bruch's membrane caused by laser photocoagulation. **B**–**E**, Fluorescence angiography images of Bl6 (**B** and **C**) or *FAAH*$^{-/-}$ mouse retina (**D** and **E**) at 3–4 min (**B** and **D**) or 6–8 min (**C** and **E**) after fluorescein injection. Red circles and a red cross denote laser lesions and the optic nerve, respectively. **F** and **G**, Statistical analysis of pixel intensity (**F**) and vascularized area (**G**) of the laser lesions at day 14 after injury and 6–8 min after fluorescein injection (n=24–27). **H**, Grading and statistical analysis of the laser lesions 14 d after injury (n=24–27); 0: no leakage, weak hyperfluorescence, 1: weak leakage, hyperfluorescent lesions not increasing in size or intensity, 2A: leakage, hyperfluorescent lesion increasing in intensity but not in size, 2B: pathological significant leakage, hyperfluorescent lesions increasing in size and intensity. **I**–**K**, Immunofluorescence staining of Bl6 choroidal flatmounts with rhodamine-conjugated lectin 24 d after injury; (**I**) overview of a Bl6 choroid, bar=100 µm, (**J**) injured area of a Bl6 choroid, bar=20 µm, (**K**) injured area of *FAAH*$^{-/-}$ choroid, bar=20 µm. **L**, Statistical analysis of lectin-stained vascular area of each lesion 24 d after injury (n=18–28). **F**, **G**, and **L**, 2-tailed unpaired Student *t* test, (**H**) χ^2 test.

such as CB receptors, TRPV1, or cyclooxygenases but via disruption of lipid rafts.

The consequences of FAAH inhibition on angiogenesis have not been investigated to date. Instead, earlier publications propose controversial findings regarding endocannabinoids, the substrates of FAAH because for them both proangiogenic as well as antiangiogenic effects mediated via classical cannabinoid receptors have been reported.[16,17] Here, we have used a different approach by using both, pharmacological blockade via the inhibitor URB597 or genetic ablation of FAAH. Interestingly, we could rule out the involvement of classic cannabinoid signaling pathways in the antiangiogenic effect of FAAH inhibition, but our results demonstrate a clear role for AEA. This finding is in accordance with earlier reports revealing that inhibition of FAAH results in AEA accumulation,[40] and that AEA and FAAH are also active in EC.[41–44] In fact, our measurements show that (1) pharmacological inhibition of FAAH results in elevated AEA levels in HUVEC, and (2) application of either AEA or the nonhydrolyzable AEA analog Met-AEA had very similar antiangiogenic effects as the FAAH inhibitor URB597. This was also the case, when investigating the gene expression pattern in EC, as gene sets for

cell cycle activity, DNA replication, integrin binding, and tissue development were found to be downregulated upon exposure to URB597 or AEA. Cell cycle progression and DNA replication were also found to be altered in response to FAAH inhibition by our TF analysis, and these have also been demonstrated to depend on various integrins[45,46] that connect the cytoskeleton with the extracellular matrix. Because integrin-binding mediates adhesion and integrin signaling was downregulated by URB597 and AEA, it is conceivable that this can result in a decrease in vascular growth, angiogenesis, and tissue development in general.[47] In particular, we found VWF, ADAM9, ADAM23, and ICAM2 as integrin-related molecules directly affecting adhesion or angiogenesis to be downregulated. In addition, earlier work has reported that the knockout of ADAM9 reduces pathological neovascularization in CNV mice.[48] This finding also underscores the protective effect of the FAAH deficiency, which we have observed in this study.

We also wondered about the underlying cellular mechanisms and noted that cell cycle regulation and matrix adhesion by integrins have been demonstrated to depend on intact lipid rafts.[49,50] These are cholesterol-rich membrane microdomains, in which various signaling molecules are assembled.[51] We found that URB597 and AEA treatment disrupted lipid rafts and this could explain altered integrin signaling and cell cycle arrest. In full accordance URB597 and AEA have been reported to inhibit proliferation of tumor cells independent from cannabinoid receptors but via a lipid raft-dependent process.[39,52] This fits to the chemical properties of endocannabinoids that can incorporate into lipid bilayers due to their amphiphilic nature and modulate the physical properties of membranes, as shown in earlier work for ion channel regulation.[53]

This lipid membrane-dependent effect of FAAH targeting may be a very promising antiangiogenic therapeutic approach. Therefore, we have tested the potential of FAAH inhibition to reduce pathological angiogenesis in vivo. A very important disease based on pathological angiogenesis is age-related macular degeneration—the leading cause of vision loss in humans worldwide. Current therapies are mainly based on VEGF antibodies exerting antiangiogenic action, but this pharmacotherapy is either not effective in some patients or loses efficacy over time.[54] Therefore, we have tested the in vivo consequences of FAAH inhibition in the laser-induced CNV model, which phenocopies key features of this widespread disease. The results clearly demonstrate that FAAH deletion prevents all signs of pathological neovascularization, whereas there were no adverse effects on physiological vascular remodeling in the heart and skeletal muscle of aged mice. This suggests that administration of FAAH inhibitors, in particular, the site-specific application in the eye via intravitreal injection, is an interesting option for the therapeutic use in age-related macular degeneration. In addition, new peripheral FAAH inhibitors without side effects in the central nervous system could enable systemic drug application for the treatment of a variety of diseases with vascular overgrowth. A limitation of the study is that in vitro concentrations of exogenously applied AEA are difficult to transfer to the in vivo situation. Nevertheless, FAAH deficiency resulted in strong antiangiogenic effects in the disease model. Future studies will have to address if FAAH inhibitors act independently from VEGF signaling and hence could be applied in an additive manner to reduce angiogenesis. Thus, our study reveals a so far unrecognized antiangiogenic mechanism, and pharmacological targeting of endocannabinoid degradation could be an interesting approach to counteract pathological angiogenesis.

ARTICLE INFORMATION

Received August 25, 2020; accepted September 23, 2021.

Affiliations

Institute of Physiology I, Life&Brain Center, Medical Faculty (S.R., S.K., B.K.F., D.W.) and Department of Ophthalmology (J.H.M., S.S.-V.), University of Bonn, Germany. Department of Systems Physiology, Institute of Physiology, Medical Faculty, Ruhr University of Bochum, Germany (M.M., D.W.). John A. Moran Eye Center, Ophthalmology & Visual Science, University of Utah, Salt Lake City (S.S.-V.). Department of Biomedical Sciences, City University of Hong Kong (H.H., L.Z., X.W.).

Acknowledgments

S. Rieck performed cell culture, immunostainings, flow cytometry analysis, analyzed data; she designed the figures and was involved in the writing of the article, S. Kilgus exerted cell culture experiments, immunostainings, flow cytometry experiments, and analyzed these data as well as aortic ring assay and choroidal neovascularization (CNV) data; J.H. Meyer generated CNV data; L. Zhao and H. Huang analyzed gene arrays; M. Matthey performed cell culture, polymerase chain reaction (PCR), and Western Blot experiments; X. Wang supervised analysis of gene arrays; S. Schmitz-Valckenberg supervised CNV experiments; B.K. Fleischmann was involved in data discussion and contributed to the writing of the article, D. Wenzel drafted the study and the article, supervised the experiments, and wrote the article. We thank Stefanie Riesenberg and Michael Hölzel (University of Bonn) for RNA isolation of human umbilical vein endothelial cells (HUVEC). We appreciate help with aortic ring assay by Sarah Vosen (University of Bonn). Moreover, we thank Stefanie Heilmann-Heimbach and Markus Nöthen (University of Bonn) for gene array measurements on the Illumina platform and Laura Bindila (University of Mainz) for liquid chromatography-multiple reaction monitoring (LC-MRM) measurements.

Sources of Funding

The project was supported by the BONFOR program of the Medical Faculty, University of Bonn, and the Deutsche Forschungsgemeinschaft DFG (WE4461/1-1) to D. Wenzel.

Disclosures

The Department of Ophthalmology, University of Bonn has received nonfinancial research funding from several imaging device manufactures, including Carl Zeiss MedicTec AG, CenterVue, Heidelberg Engineering, and Optos, outside the submitted work. S. Schmitz-Valckenberg reports grants from Acucela and Katairo, grants and personal fees from Alcon/Novartis, Allergan, Bayer, Bioeq/Formycon and Roche/Genentech, grants, personal fees and nonfinancial support from Carl Zeiss MediTec AG, grants and nonfinancial support from Centervue and Heidelberg Engineering, personal fees from Galimedix and Oxurion as well as nonfinancial support from Optos, outside the submitted work. The other authors report no conflicts.

Supplementary Materials

Online Figures I–X
Online Tables I–II

REFERENCES

1. Smith SK. Angiogenesis and reproduction. *BJOG*. 2001;108:777–783. doi: 10.1111/j.1471-0528.2001.00211.x
2. Mecklenburg L, Tobin DJ, Müller-Röver S, Handjiski B, Wendt G, Peters EM, Pohl S, Moll I, Paus R. Active hair growth (anagen) is associated with angiogenesis. *J Invest Dermatol*. 2000;114:909–916. doi: 10.1046/j.1523-1747.2000.00954.x
3. Tonnesen MG, Feng X, Clark RA. Angiogenesis in wound healing. *J Investig Dermatol Symp Proc*. 2000;5:40–46. doi: 10.1046/j.1087-0024.2000.00014.x
4. Krupinski J, Kaluza J, Kumar P, Kumar S, Wang JM. Role of angiogenesis in patients with cerebral ischemic stroke. *Stroke*. 1994;25:1794–1798. doi: 10.1161/01.str.25.9.1794
5. Crawford TN, Alfaro DV 3rd, Kerrison JB, Jablon EP. Diabetic retinopathy and angiogenesis. *Curr Diabetes Rev*. 2009;5:8–13. doi: 10.2174/157339909787314149
6. Heidenreich R, Röcken M, Ghoreschi K. Angiogenesis drives psoriasis pathogenesis. *Int J Exp Pathol*. 2009;90:232–248. doi: 10.1111/j.1365-2613.2009.00669.x
7. Robinson ES, Khankin EV, Karumanchi SA, Humphreys BD. Hypertension induced by vascular endothelial growth factor signaling pathway inhibition: mechanisms and potential use as a biomarker. *Semin Nephrol*. 2010;30:591–601. doi: 10.1016/j.semnephrol.2010.09.007
8. Wenzel D, Schmidt A, Reimann K, Hescheler J, Pfitzer G, Bloch W, Fleischmann BK. Endostatin, the proteolytic fragment of collagen XVIII, induces vasorelaxation. *Circ Res*. 2006;98:1203–1211. doi: 10.1161/01.RES.0000219899.93384.ed
9. Wenzel D, Matthey M, Bindila L, Lerner R, Lutz B, Zimmer A, Fleischmann BK. Endocannabinoid anandamide mediates hypoxic pulmonary vasoconstriction. *Proc Natl Acad Sci USA*. 2013;110:18710–18715. doi: 10.1073/pnas.1308130110
10. Williams CM, Kirkham TC. Anandamide induces overeating: mediation by central cannabinoid (CB1) receptors. *Psychopharmacology (Berl)*. 1999;143:315–317. doi: 10.1007/s002130050953
11. Mallet PE, Beninger RJ. The cannabinoid CB1 receptor antagonist SR141716A attenuates the memory impairment produced by delta9-tetrahydrocannabinol or anandamide. *Psychopharmacology (Berl)*. 1998;140:11–19. doi: 10.1007/s002130050733
12. Martin BR, Lichtman AH. Cannabinoid transmission and pain perception. *Neurobiol Dis*. 1998;5(6 pt B):447–461. doi: 10.1006/nbdi.1998.0218
13. Randall MD, Kendall DA. Endocannabinoids: a new class of vasoactive substances. *Trends Pharmacol Sci*. 1998;19:55–58. doi: 10.1016/s0165-6147(97)01161-9
14. Hillard CJ. Endocannabinoids and vascular function. *J Pharmacol Exp Ther*. 2000;294:27–32.
15. Wahn H, Wolf J, Kram F, Frantz S, Wagner JA. The endocannabinoid arachidonyl ethanolamide (anandamide) increases pulmonary arterial pressure via cyclooxygenase-2 products in isolated rabbit lungs. *Am J Physiol Heart Circ Physiol*. 2005;289:H2491–H2496. doi: 10.1152/ajpheart.00718.2005
16. Pisanti S, Picardi P, Prota L, Proto MC, Laezza C, McGuire PG, Morbidelli L, Gazzerro P, Ziche M, Das A, et al. Genetic and pharmacologic inactivation of cannabinoid CB1 receptor inhibits angiogenesis. *Blood*. 2011;117:5541–5550. doi: 10.1182/blood-2010-09-307355
17. Pisanti S, Borselli C, Oliviero O, Laezza C, Gazzerro P, Bifulco M. Antiangiogenic activity of the endocannabinoid anandamide: correlation to its tumor-suppressor efficacy. *J Cell Physiol*. 2007;211:495–503. doi: 10.1002/jcp.20954
18. Herz K, Heinemann JC, Hesse M, Ottersbach A, Geisen C, Fuegemann CJ, Röll W, Fleischmann BK, Wenzel D. Live monitoring of small vessels during development and disease using the flt-1 promoter element. *Basic Res Cardiol*. 2012;107:257. doi: 10.1007/s00395-012-0257-5
19. Rieck S, Heun Y, Heidsieck A, Mykhaylyk O, Pfeifer A, Gleich B, Mannell H, Wenzel D. Local anti-angiogenic therapy by magnet-assisted downregulation of SHP2 phosphatase. *J Control Release*. 2019;305:155–164. doi: 10.1016/j.jconrel.2019.05.031
20. Wenzel D, Rieck S, Vosen S, Mykhaylyk O, Trueck C, Eberbeck D, Trahms L, Zimmermann K, Pfeifer A, Fleischmann BK. Identification of magnetic nanoparticles for combined positioning and lentiviral transduction of endothelial cells. *Pharm Res*. 2012;29:1242–1254. doi: 10.1007/s11095-011-0657-5
21. Vosen S, Rieck S, Heidsieck A, Mykhaylyk O, Zimmermann K, Bloch W, Eberbeck D, Plank C, Gleich B, Pfeifer A, et al. Vascular repair by circumferential cell therapy using magnetic nanoparticles and tailored magnets. *ACS Nano*. 2016;10:369–376. doi: 10.1021/acsnano.5b04996
22. Vosen S, Rieck S, Heidsieck A, Mykhaylyk O, Zimmermann K, Plank C, Gleich B, Pfeifer A, Fleischmann BK, Wenzel D. Improvement of vascular function by magnetic nanoparticle-assisted circumferential gene transfer into the native endothelium. *J Control Release*. 2016;241:164–173. doi: 10.1016/j.jconrel.2016.09.024
23. Malan D, Wenzel D, Schmidt A, Geisen C, Raible A, Bölck B, Fleischmann BK, Bloch W. Endothelial beta1 integrins regulate sprouting and network formation during vascular development. *Development*. 2010;137:993–1002. doi: 10.1242/dev.045377
24. Schmidt A, Wenzel D, Thorey I, Sasaki T, Hescheler J, Timpl R, Addicks K, Werner S, Fleischmann BK, Bloch W. Endostatin influences endothelial morphology via the activated ERK1/2-kinase endothelial morphology and signal transduction. *Microvasc Res*. 2006;71:152–162. doi: 10.1016/j.mvr.2006.01.001
25. Matthey M, Roberts R, Seidinger A, Simon A, Schröder R, Kuschak M, Annala S, König GM, Müller CE, Hall IP, et al. Targeted inhibition of Gq signaling induces airway relaxation in mouse models of asthma. *Sci Transl Med*. 2017;9:eaag2288. doi: 10.1126/scitranslmed.aag2288
26. Welschoff J, Matthey M, Wenzel D. RGD peptides induce relaxation of pulmonary arteries and airways via β3-integrins. *FASEB J*. 2014;28:2281–2292. doi: 10.1096/fj.13-246348
27. Wenzel D, Knies R, Matthey M, Klein AM, Welschoff J, Stolle V, Sasse P, Röll W, Breuer J, Fleischmann BK. beta(2)-adrenoceptor antagonist ICI 118,551 decreases pulmonary vascular tone in mice via a G(i/o) protein/nitric oxide-coupled pathway. *Hypertension*. 2009;54:157–163. doi: 10.1161/HYPERTENSIONAHA.109.130468
28. Ritchie ME, Phipson B, Wu D, Hu Y, Law CW, Shi W, Smyth GK. limma powers differential expression analyses for RNA-sequencing and microarray studies. *Nucleic Acids Res*. 2015;43:e47. doi: 10.1093/nar/gkv007
29. Subramanian A, Tamayo P, Mootha VK, Mukherjee S, Ebert BL, Gillette MA, Paulovich A, Pomeroy SL, Golub TR, Lander ES, et al. Gene set enrichment analysis: a knowledge-based approach for interpreting genome-wide expression profiles. *Proc Natl Acad Sci USA*. 2005;102:15545–15550. doi: 10.1073/pnas.0506580102
30. Wang X, Terfve C, Rose JC, Markowetz F. HTSanalyzeR: an R/Bioconductor package for integrated network analysis of high-throughput screens. *Bioinformatics*. 2011;27:879–880. doi: 10.1093/bioinformatics/btr028
31. Meyer JH, Cunea A, Licha K, Welker P, Sonntag-Bensch D, Wafula P, Dernedde J, Fimmers R, Holz FG, Schmitz-Valckenberg S. In vivo imaging of fluorescent probes linked to antibodies against human and rat vascular endothelial growth factor. *Invest Ophthalmol Vis Sci*. 2016;57:759–770. doi: 10.1167/iovs.15-18118
32. Yu HG, Liu X, Kiss S, Connolly E, Gragoudas ES, Michaud NA, Bulgakov OV, Adamian M, DeAngelis MM, Miller JW, et al. Increased choroidal neovascularization following laser induction in mice lacking lysyl oxidase-like 1. *Invest Ophthalmol Vis Sci*. 2008;49:2599–2605. doi: 10.1167/iovs.07-1508
33. Fischer AH, Jacobson KA, Rose J, Zeller R. Hematoxylin and eosin staining of tissue and cell sections. *CSH Protoc*. 2008;2008:pdb prot4986. doi: 10.1101/pdb.prot4986
34. Starke RD, Ferraro F, Paschalaki KE, Dryden NH, McKinnon TA, Sutton RE, Payne EM, Haskard DO, Hughes AD, Cutler DF, et al. Endothelial von Willebrand factor regulates angiogenesis. *Blood*. 2011;117:1071–1080. doi: 10.1182/blood-2010-01-264507
35. Mygind KJ, Schwarz J, Sahgal P, Ivaska J, Kveiborg M. Loss of ADAM9 expression impairs β1 integrin endocytosis, focal adhesion formation and cancer cell migration. *J Cell Sci*. 2018;131:jcs205393. doi: 10.1242/jcs.205393
36. Cal S, Freije JM, López JM, Takada Y, López-Otín C. ADAM 23/MDC3, a human disintegrin that promotes cell adhesion via interaction with the alphavbeta3 integrin through an RGD-independent mechanism. *Mol Biol Cell*. 2000;11:1457–1469. doi: 10.1091/mbc.11.4.1457
37. Huang MT, Mason JC, Birdsey GM, Amsellem V, Gerwin N, Haskard DO, Ridley AJ, Randi AM. Endothelial intercellular adhesion molecule (ICAM)-2 regulates angiogenesis. *Blood*. 2005;106:1636–1643. doi: 10.1182/blood-2004-12-4716
38. Kanehisa M, Goto S. KEGG: kyoto encyclopedia of genes and genomes. *Nucleic Acids Res*. 2000;28:27–30. doi: 10.1093/nar/28.1.27
39. Hamtiaux L, Hansoulle L, Dauguet N, Muccioli GG, Gallez B, Lambert DM. Increasing antiproliferative properties of endocannabinoids in N1E-115 neuroblastoma cells through inhibition of their metabolism. *PLoS One*. 2011;6:e26823. doi: 10.1371/journal.pone.0026823
40. Pacher P, Bátkai S, Osei-Hyiaman D, Offertáler L, Liu J, Harvey-White J, Brassai A, Járai Z, Cravatt BF, Kunos G. Hemodynamic profile, responsiveness to anandamide, and baroreflex sensitivity of mice lacking fatty acid

amide hydrolase. *Am J Physiol Heart Circ Physiol*. 2005;289:H533–H541. doi: 10.1152/ajpheart.00107.2005
41. Maccarrone M, Bari M, Lorenzon T, Bisogno T, Di Marzo V, Finazzi-Agrò A. Anandamide uptake by human endothelial cells and its regulation by nitric oxide. *J Biol Chem*. 2000;275:13484–13492. doi: 10.1074/jbc.275.18.13484
42. Maccarrone M, Bari M, Battista N, Finazzi-Agrò A. Estrogen stimulates arachidonoylethanolamide release from human endothelial cells and platelet activation. *Blood*. 2002;100:4040–4048. doi: 10.1182/blood-2002-05-1444
43. Deutsch DG, Goligorsky MS, Schmid PC, Krebsbach RJ, Schmid HH, Das SK, Dey SK, Arreaza G, Thorup C, Stefano G, et al. Production and physiological actions of anandamide in the vasculature of the rat kidney. *J Clin Invest*. 1997;100:1538–1546. doi: 10.1172/JCI119677
44. Opitz CA, Rimmerman N, Zhang Y, Mead LE, Yoder MC, Ingram DA, Walker JM, Rehman J. Production of the endocannabinoids anandamide and 2-arachidonoylglycerol by endothelial progenitor cells. *FEBS Lett*. 2007;581:4927–4931. doi: 10.1016/j.febslet.2007.09.032
45. Schwartz MA, Assoian RK. Integrins and cell proliferation: regulation of cyclin-dependent kinases via cytoplasmic signaling pathways. *J Cell Sci*. 2001;114(pt 14):2553–2560.
46. Moreno-Layseca P, Streuli CH. Signalling pathways linking integrins with cell cycle progression. *Matrix Biol*. 2014;34:144–153. doi: 10.1016/j.matbio.2013.10.011
47. Hynes RO. Cell-matrix adhesion in vascular development. *J Thromb Haemost*. 2007;5(Suppl 1):32–40. doi: 10.1111/j.1538-7836.2007.02569.x
48. Guaiquil V, Swendeman S, Yoshida T, Chavala S, Campochiaro PA, Blobel CP. ADAM9 is involved in pathological retinal neovascularization. *Mol Cell Biol*. 2009;29:2694–2703. doi: 10.1128/MCB.01460-08
49. Leitinger B, Hogg N. The involvement of lipid rafts in the regulation of integrin function. *J Cell Sci*. 2002;115(pt 5):963–972.
50. Gagnoux-Palacios L, Dans M, van't Hof W, Mariotti A, Pepe A, Meneguzzi G, Resh MD, Giancotti FG. Compartmentalization of integrin alpha6beta4 signaling in lipid rafts. *J Cell Biol*. 2003;162:1189–1196. doi: 10.1083/jcb.200305006
51. Simons K, Toomre D. Lipid rafts and signal transduction. *Nat Rev Mol Cell Biol*. 2000;1:31–39. doi: 10.1038/35036052
52. DeMorrow S, Glaser S, Francis H, Venter J, Vaculin B, Vaculin S, Alpini G. Opposing actions of endocannabinoids on cholangiocarcinoma growth: recruitment of Fas and Fas ligand to lipid rafts. *J Biol Chem*. 2007;282:13098–13113. doi: 10.1074/jbc.M608238200
53. Medeiros D, Silva-Gonçalves LC, da Silva AM, Dos Santos Cabrera MP, Arcisio-Miranda M. Membrane-mediated action of the endocannabinoid anandamide on membrane proteins: implications for understanding the receptor-independent mechanism. *Sci Rep*. 2017;7:41362. doi: 10.1038/srep41362
54. Yang S, Zhao J, Sun X. Resistance to anti-VEGF therapy in neovascular age-related macular degeneration: a comprehensive review. *Drug Des Devel Ther*. 2016;10:1857–1867. doi: 10.2147/DDDT.S97653